Laser Thinning for Monolayer Graphene Formation: Heat Sink and Interference Effect

Gang Hee Han,[†] Seung Jin Chae,[†] Eun Sung Kim,[†] Fethullah Güneş,[†] Il Ha Lee,[†] Sang Won Lee,[†] Si Young Lee,[†] Seong Chu Lim,[†] Hae Kyung Jeong,[‡] Mun Seok Jeong,[§] and Young Hee Lee[†,*]

[†]BK21 Physics Division, Department of Energy Science, Center for Nanotubes and Nanostructured Composites, and Sungkyunkwan Advanced Institute of Nanotechnology, Sungkyunkwan University, Suwon 440-746, Korea, [‡]Department of Physics, Daegu University, Jillyang, Gyeongsan, Gyeongbuk 712-714, Korea, and [§]Advanced Photonics Research Institute, Gwangju Institute of Science and Technology, Oryong-dong, Buk-gu, Gwangju 500-712, Korea

ABSTRACT Despite the availability of large-area graphene synthesized by chemical vapor deposition (CVD), the control of a uniform monolayer graphene remained challenging. Here, we report a method of acquiring monolayer graphene by laser irradiation. The accumulation of heat on graphene by absorbing light, followed by oxidative burning of upper graphene layers, which strongly relies on the wavelength of light and optical parameters of the substrate, was *in situ* measured by the G-band shift in Raman spectroscopy. The substrate plays a crucial role as a heat sink for the bottom monolayer graphene, resulting in no burning or etching. Oscillatory thinning behavior dependent on the substrate oxide thickness was evaluated by adopting a simple Fresnel's equation. This paves the way for future research in utilizing monolayer graphene for high-speed electronic devices.

KEYWORDS: graphene · laser etching · monolayer · Fresnel's equation

Despite recent advances in the synthesis of large-area graphene by using various substrates, such as Ni and Cu,[1−6] few-layered graphene or graphene islands on monolayer graphene have been often observed instead of monolayer graphene with high uniformity. Several approaches have been tried for graphene etching: heat-induced etching by oxygen,[7] cutting graphene by carbon-soluble metals,[8,9] and an e-beam lithography assisted technique.[10,11] Previously, graphite oxide cutting by a laser has been reported.[12] Nevertheless, none of these approaches provides a means of obtaining monolayer graphene that is scientifically and technologically relevant graphene. The absence of such an approach hampers not only discovery of new science but also pushing the carrier mobility to the limit.

Etching of graphene, in general, involves a complicated heat transfer and dissipation mechanism. Incident light is absorbed, in part, by the graphene layers and transmitted through the layers, which is reflected at the boundary of the substrate. In the case of the Si substrate, two boundaries are formed at the top of the SiO_2 layer and at the bottom of the Si substrate. Light is reflected at these boundaries, resulting in light absorbance in the graphene layers again. The amount of reflected light strongly relies on the refractive index and thickness of oxide and Si. As a consequence of light absorption following such complicated multiple reflections, the temperature of the graphene layer is expected to increase. Competition of heat accumulation by light absorption and heat dissipation through planar graphene layers and the perpendicular direction to the substrate determines the temperature of graphene layers.

The purpose of this paper is to design a method of obtaining a monolayer graphene by laser irradiation. We introduced few graphene layers on a SiO_2/Si substrate, which was subjected to laser irradiation. Whereas the top graphene layers were etched completely by scanning laser beams, the bottom monolayer graphene remained unetched. This was explained by the heat accumulation on the upper graphene layers by light absorption, whereas the SiO_2/Si substrate plays a crucial role as a heat sink for the monolayer graphene to remain unetched. The etching ability was controlled by the oxide layer thickness, congruent with a prediction from Fresnel's equation. Because of an efficient role of the Si substrate as a heat sink, the undesirable damage of defect formation was prevented.

RESULTS AND DISCUSSION

Two types of graphene layers were used as substrates for laser etching in this study:

*Address correspondence to leeyoung@skku.edu.

Received for review October 5, 2010 and accepted December 09, 2010.

Published online December 21, 2010.
10.1021/nn1026438

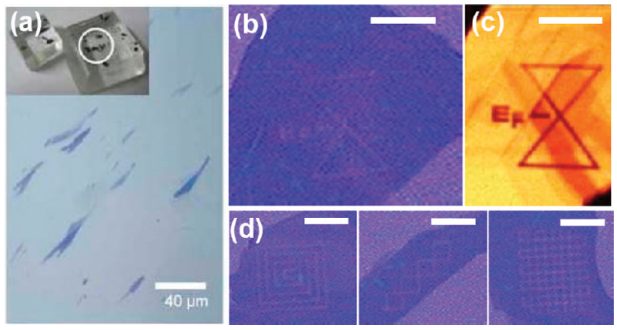

Figure 1. Laser etching and various patterns of graphene. (a) A PDMS mold with HOPG flakes (inset) marked by white circles is shown. Graphene flakes were stamped on silicon/silicon dioxide. (b, c) Optical microscopy image and confocal Raman spectroscopy with a laser excitation energy of 532 nm at a power of <1 mW and a beam diameter of ~350 nm, integrated over the G-band (1540−1620 cm^{-1}). Black solid lines indicate the reduction of the G-band intensity, that is, the disappearance of HOPG. (d) Various patterns formed by laser etching. The scale bars of (b−d) are 5 μm.

highly oriented pyrolytic graphite (HOPG) and large-area graphene. HOPG was randomly transferred onto a SiO_2/Si substrate by using a polydimethylsiloxane (PDMS) mold (Supporting Information, Figure S1). Large-area graphene was synthesized by thermal chemical vapor deposition (TCVD) and transferred by a fishing method onto the SiO_2/Si substrate.[1,2,4−6] Figure 1a shows the PDMS stamp with HOPG flakes on it (inset). Clean HOPG flakes are easily and randomly transferred on the wafer.

Confocal Raman spectroscopy (WITec, 532 nm wavelength, TEM_{00} mode) was used to etch away graphitic layers with a reasonable laser power density of 8×10^{-4} mW/nm^2. The laser was operated at a scan rate of 0.9−10 μm/s along the plane to create a patterned etching. The mechanically cleaved samples had 4−7 graphene layers. Various optical patterns provided in Figure 1b,d clearly show evidence of etching of the graphene layers during laser scanning. As will be discussed later, monolayer graphene remained unetched, independent of the thickness of the original sample. After laser patterning, the whole area was scanned again with a reduced power density for confocal Raman mapping of the G-band (Figure 1c). The dark solid lines depicting the energy band of graphene indicate the disappearance of graphitic layers resulting from the reduction of the G-band intensity, but not zero intensity, whereas the bright area indicates that graphitic layers remained intact during scanning. Chessboard-like and spider-web-like patterns were also demonstrated (Figure 1d). The same pattern phenomena were also observed in the CVD-grown samples on the Ni substrate (Supporting Information, Figure S2). The uniformity of the etched graphene compared with the rough surface of the CVD-grown graphene was also demonstrated by atomic force microscopy (AFM) (Supporting Information, Figure S3).

By choosing the proximate scanning interval condition, the continuous removal of graphitic layers was achieved (Figure 2). The etched dark area in Figure 2a (right) is an indication of reduction of the G-band intensity. Although the thickness of the HOPG flakes is slightly different from place to place, indicated by the contrast of G-band mapping in Figure 2a (left), the uniformity of the etched dark area demonstrates efficiency of the laser thinning. Therefore, the thinning of graphitic layers is independent of the thickness of graphitic layers. The transferred HOPG was characterized by the G′-band near 2726 cm^{-1}, whose intensity was relatively low compared with that of the G-band (Figure 2b, left). This is equivalent to approximately 4−5

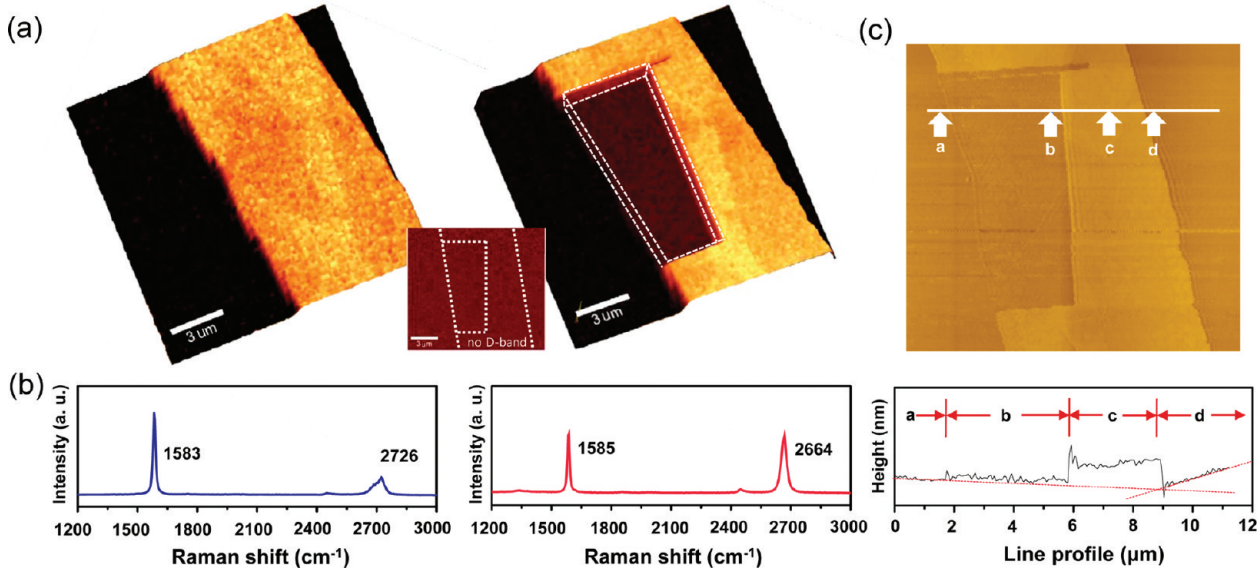

Figure 2. Confocal Raman mapping of the G-band and Raman shift before and after graphene thinning. (a) Confocal Raman mapping of the G-band (1540−1620 cm^{-1}) before (left) and after (right) thinning. The inset shows D-band (1300−1400 cm^{-1}) mapping. (b) Raman shift taken in the unthinned region (left) and that in the thinned region (right). The distinction of the thinned region is marked by dashed lines. The peak position of the G′-band is downshifted after thinning. (c) AFM images of the same sample of the etched area and the related height profile. The graphene layer remained after etching with a thickness of 0.8 ± 0.2 nm.

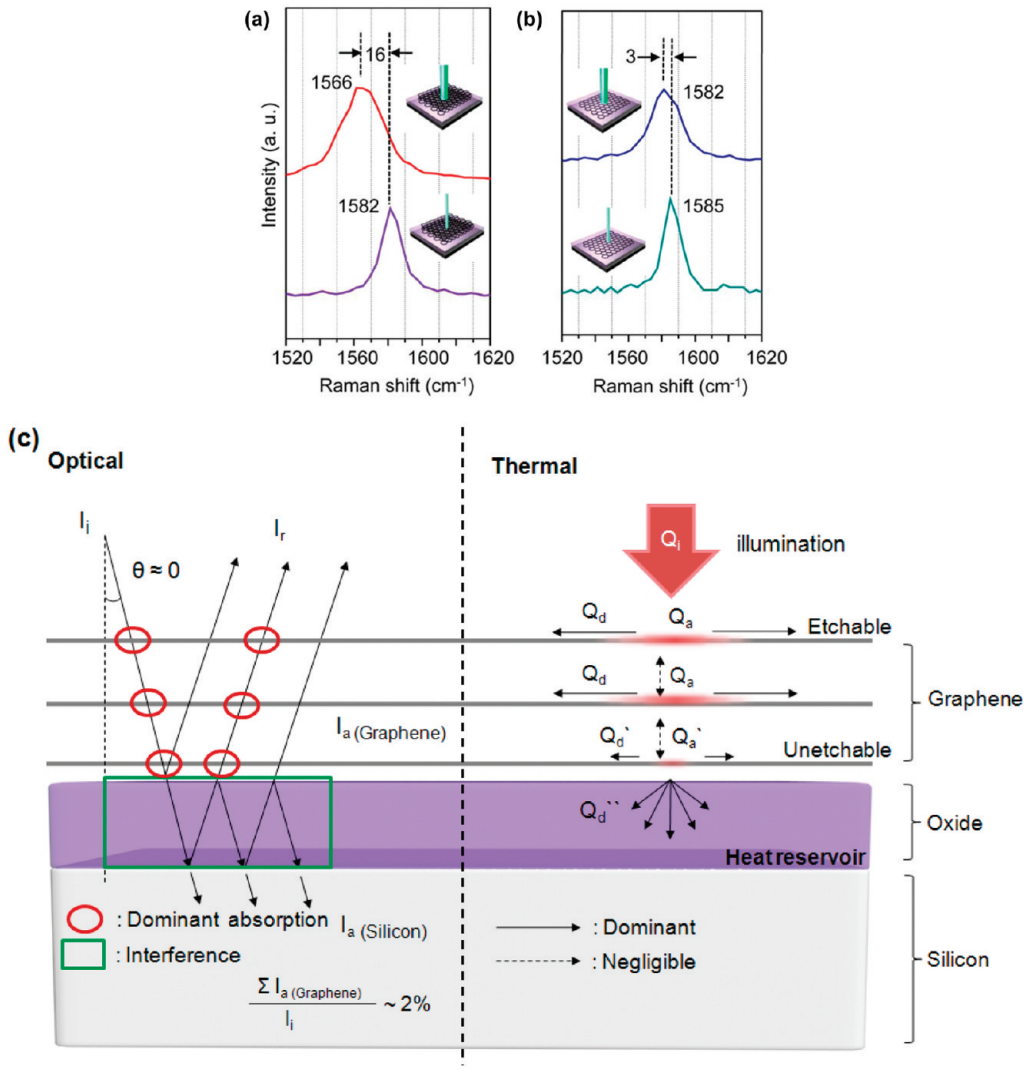

Figure 3. Phonon softening by accumulated heat with a schematic of heat accumulation in graphene with different thicknesses. Each graphene layer absorbs light and thus becomes heated. The light is reflected from the bottom substrate. The Si substrate acts as a heat sink. The temperature increase was monitored by *in situ* measurements of the G-band shift using confocal Raman spectroscopy. The lower (upper) curve in the Raman spectra was obtained from a low (high)-power laser. Thicker graphene layers (a) absorb more heat than thinner ones (b). A detailed schematic is shown in (c)

graphitic layers as compared to the previous Raman spectroscopy[13] and optical contrast[14−23] observations. However, the etched dark area revealed a G′-band with a relatively strong Lorentzian intensity near 2664 cm^{-1} (Figure 2b, right), which is equivalent to those of monolayer graphene.[13] This demonstrates that few-layer graphene can be reduced to monolayer graphene under a reasonable power density range. During this etching process, no appreciable D-band was developed in the remaining monolayer graphene; that is, no clear distinction in the D-band mapping between the scanned and the unscanned regions was visible (inset). Figure 2c shows AFM images of the same sample in the vicinity of the etched area and the related height profile. This clearly demonstrates that the graphene layer remained unchanged after etching with a thickness of 0.8 ± 0.2 nm, indicating a monolayer graphene.[24]

We demonstrate a Raman shift upon local heating for two cases of graphene layers; thick layers (4−5 layer) and monolayer for Figure 3a,b, respectively. The incident laser is absorbed by graphene layers. The local temperature increase was monitored by *in situ* confocal Raman spectroscopy. Phonon softening and thermal broadening of the G-band are expected from the local temperature increase. The increased temperature can be evaluated numerically by the G-band peak shift; $T = [\omega(T) - \omega(T_1)]/\chi$, where $\omega(T)$ is the G-band shift at temperature T, $\omega(T_1)$ is the G-band shift at room temperature from an extrapolated method, and χ is 0.011 cm^{-1}/°C and varies slightly with the number of graphene layers.[25,26] When thick graphene (4−5 layers) was exposed to the laser with a high power (Figure 3a), the G-band was downshifted by 16 cm^{-1}. This gives rise to a local temperature increase of ~1450 °C. The full width at half-maximum of the G-band was increased

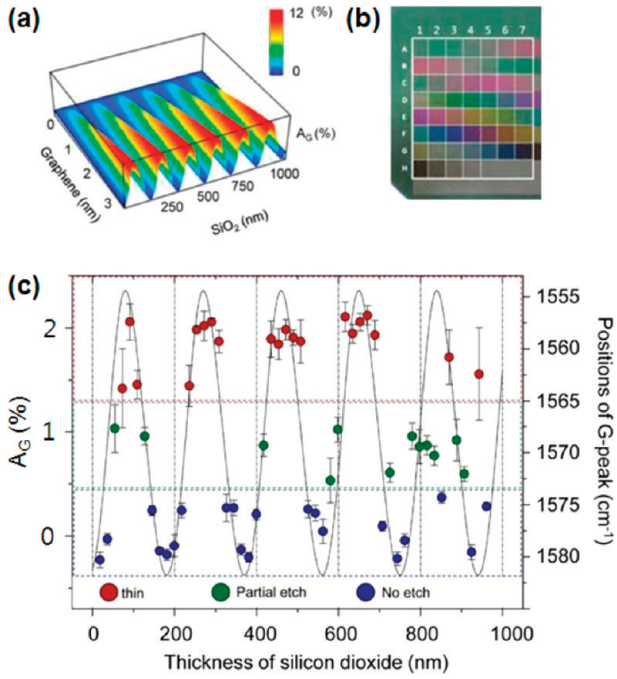

Figure 4. Dependence of laser thinning on the substrate and graphene thickness. (a) Three-dimensional plot of absorbance derived from Fresnel's equation as a function of the thickness of the silicon diode and graphene layers. (b) Optical image of the SiO_2 substrate with different thicknesses prepared by BOE etching. The color represents SiO_2 layers of different thicknesses. (c) Comparison of the laser thinning effect from experiments. The solid line represents theoretical absorbance on bilayer graphene with various thicknesses of SiO_2 layers calculated from Fresnel's equation. The related experimental data for the G-band shift with 4−7 layers of graphene were also plotted with symbols. Three regions in red, green, and blue indicate the etched, partially etched, and not etched regions, respectively.

by 17 cm^{-1}, indicating thermal broadening. Because this experiment was performed under ambient conditions, the thick graphene layers were burnt out by an instantaneous (exposure time = 36 ms) oxidative etching process. The burning temperature of a graphitic flake is 730 °C, as measured from thermogravimetric analysis (Supporting Information, Figure S4). In contrast, for monolayer graphene (Figure 3b), high-power laser irradiation resulted in only a 3 cm^{-1} downshift in the G-band peak position, where only a 2−300 °C increase of temperature is expected. During the course of our experiments, the temperature of the Si substrate remained unchanged, implying efficient heat dissipation through the Si substrate. The heavy Si substrate plays a role as a heat sink in this case.

From the optical and thermal points of view (Figure 3c), for the simplest case of normal incident light, the incident light is absorbed on graphene layers. The transmitted light through the graphene layers reaches the top of the SiO_2 layer and is partially reflected and transmitted. The transmitted light that reaches the Si substrate is again partially reflected and absorbed. The reflected light from the two interfaces is then absorbed on the graphene layers again. The circles indicate dominant absorption points. As a consequence, the light absorbed by the graphene layers generates local heating on the graphene plane. The generated heat then propagates along the basal plane of graphene because of high thermal conductivity. The heat dissipation perpendicular to the graphene layer is lower than the planar direction by an order of 10^4 (ref 27). Therefore, the heat dissipation is dominant along the planar direction. A recent report explains that the silicon dioxide substrate suppresses the thermal conductivity of graphene in the planar direction by phonon leakage or additional phonon scattering at the graphene−oxide interface.[28] This provides the chances of graphene to increase the temperature by satisfying the condition $Q_a > Q_d$, where Q_a is absorbed heat and Q_d is dissipated heat in graphene, and the temperature in the graphene will increase. In the case of the bottom monolayer graphene, the situation is completely different due to the presence of the substrate. It has been well known that a heat conduction network is well established between the bottom graphene layer and the substrate.[29] In this case, $Q_a' \ll Q_d' + Q_d''$, where Q_d'' is the dissipated heat through the substrate. Q_d'' can be easily dissipated due to heavy mass, which acts as a heat reservoir. As a consequence, the temperature of the bottom graphene layer remains unaltered.

A series of experiments with different numbers of graphene layers and thicknesses of oxide in the substrate were performed to evaluate the efficacy of thinning. Regardless of the thickness of graphene, monolayer graphene was always obtained. The temperature of graphene layers is proportional to the absorbance of the incident light. The absorbance can, in principle, be described by classical optics theory.[18] The absorbance of graphene, A_G, can be written as A_G (λ, d_G, n_G, d_{SiO_2}, n_{SiO_2}, d_{Si}, n_{Si}), where λ is the wavelength of incident light; d_G, d_{SiO_2}, and d_{Si} are the respective thicknesses of graphene, SiO_2, and Si, respectively; and n_G, n_{SiO_2}, and n_{Si} are the refractive indices of graphene, SiO_2, and Si, respectively. For a given laser power and infinite thickness Si substrate, the reflectance can be described by Fresnel's equation with and without graphene layers. This equation is valid with a graphene layer thickness less than the skin depth. The total amount of absorbed light on graphene is then defined by the difference of reflectance, $A_G = (R_{sub} - R_{G/sub})$, where R_{sub} and $R_{G/sub}$ are the reflectance in the absence and presence of graphene layers on the Si substrate, respectively (Supporting Information, eq S5). A three-dimensional graph for the number of graphene layers and the corresponding oxide layer thickness is also provided in Figure 4a. The total absorption of incident light increased gradually as the number of graphene layers increased. To experimentally demonstrate the dependence of the oxide layer thickness on the etching of graphene layers, we prepared the substrate with about 50 different oxide layer thicknesses (Figure 4b) using a buffered oxide etchant (BOE). The solid line in Figure 4c indicates A_G

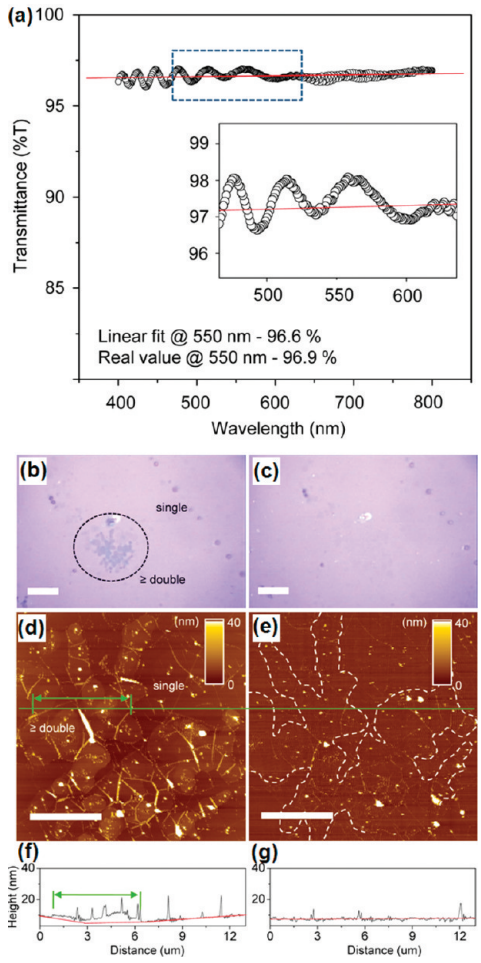

Figure 5. Transmittance of monolayer dominant graphene and laser thinning. (a) Graphene synthesized from Cu foil was transferred onto the PET substrate after Cu etching. Because of the formation of small graphene islands and PMMA beads that were used for transfer of graphene, transmittance was lower than 97.7% (ideal value) of monolayer graphene. (b, c) Optical images of graphene before and after laser thinning. Graphene on Cu foil was transferred onto the SiO_2/Si wafer, followed by laser irradiation. The scale bar is 10 μm. The circled area in (b) is scanned by AFM. (d, e) AFM images of graphene before and after laser thinning. The height profile was provided along the green line. (f) The average height of the islands was ~5 nm. (g) The islands were removed after thinning, and the remaining graphene layer was well-flattened. The dashed line provides the trace of the graphene islands before thinning. The scale bar in the AFM image is 4 μm.

calculated from Fresnel's equation as a function of oxide layer thickness for three graphene layers. A periodic repetition with the oxide layer thickness is clearly observed, mainly due to the reflection from the Si substrate. The graphene layer was prepared on this substrate, and laser etching was conducted while measuring Raman spectra simultaneously. The Raman shift follows the A_G curve well, as shown in Figure 4c. The amount of etching observed on the graphene layers was categorized as follows: (i) etched (upper), (ii) partially etched (middle), and (iii) not etched (lower). The lower-bound temperatures of the first and second region are ~1400 and ~900 °C, respectively. Graphene layers are partially etched between 850 and 1400 °C, consistent with the burning temperature of graphite powder near 730 °C. Because the duration time of our laser etching process was short due to the fast scan rate we used, a relatively high temperature was required to completely burn up the graphene layers. Accordingly, at temperatures below 700 °C, no etching was observed. The existence of the three etching states agrees well with the theoretical predictions of the A_G curve.

We now demonstrate that the laser thinning effect can be utilized to generate uniform monolayer graphene from CVD-grown graphene (Figure 5a). To synthesize graphene, Cu foil was used. The details have been described elsewhere.[6,30] The transmittance from the graphene transferred onto the polyethylene terephthalate (PET) substrate was 96.6% at 550 nm. This is slightly lower than the ideal[31,32] transmittance (97.7%) of monolayer graphene. This was attributed to the formation of small graphene islands that were several layers thick (Figure 5b). After laser irradiation, thick islands or clusters were completely removed, as shown in the optical image (Figure 5c). The AFM image also shows a similar thinning behavior (Figure 5d,e). The surface was cleaned and flattened, as shown in the height profile (Figure 5f,g). No appreciable D-band was developed after etching, as confirmed in the D-band mapping profile (Supporting Information, Figure S6).

CONCLUSION

We have developed the method of acquiring monolayer graphene by laser irradiation. The etching effect strongly relies on the wavelength of the laser, the refractive index, and the thickness of the oxide. The obtained monolayer graphene keeps its high crystallinity due to the presence of the substrate as a heat reservoir. In general, the high-power laser could be a drawback for Raman spectroscopy studies. However, the damage on graphene can be prevented by choosing appropriate substrates, as demonstrated here. In conclusion, this simple method of obtaining monolayer graphene opens the possibility for integration of electronic devices in a large area.

EXPERIMENTAL SECTION

HOPG/SiO_2 Wafer. HOPG was purchased from General Electric Advanced Ceramic (GE, ZYH grade). To prepare the PDMS mold, a Sylgard 184 silicon elastomer kit was used. The mixing ratio between the base/curing agent was 10:1. After curing (at 70 °C) for 3 h, the graphitic flake was detached from HOPG and stamped on the silicon wafers with various thicknesses of the silicon oxide layers. Details are as described in the Supporting Information (S1).

CVD Graphene/SiO_2 Wafer. Graphene was synthesized in an atmospheric CVD (5 cm in diameter) chamber. The chamber was

heated to 1030 °C with 500 sccm Ar and 200 sccm H_2. CH_4 (5 sccm) was then introduced for 5 min. After natural cooling to room temperature in the same atmosphere, graphene was transferred to the Si wafer by the PMMA assisted method.[6]

Laser Etching. For thinning, graphene samples were scanned by confocal Raman spectroscopy (WITec, 532 nm wavelength, TEM_{00} mode, ×100 lens, 0.9 N.A.) with high power (>60 mW). A scanning speed of 0.9−10 μm/s was applied along the plane. In this case, the speed of the scanning was not critical.

Acknowledgment. This research was supported by the Star-Faculty Program, World Class University (WCU) Program (2008-000-10029-0), and the International Research & Development Program (2010-00429) of the National Research Foundation of Korea (NRF) funded by the Ministry of Education, Science and Technology (MEST) of Korea.

Supporting Information Available: Details of sample preparation, laser patterning on the CVD-grown sample, laser thinning observed from the ATM image, burning temperature estimation of graphene by TGA, and equations showing the calculation of A_G. This material is available free of charge *via* the Internet at http://pubs.acs.org.

REFERENCES AND NOTES

1. Reina, A.; Jia, X.; Ho, J.; Nezich, D.; Son, H.; Bulovic, V.; Dresselhaus, M. S.; Kong, J. Large Area, Few-Layer Graphene Films on Arbitrary Substrates by Chemical Vapor Deposition. *Nano Lett.* **2009**, *9*, 30–35.
2. Kim, K. S.; Zhao, Y.; Jang, H.; Lee, S. Y.; Kim, J. M.; Kim, K. S.; Ahn, J.; Kim, P.; Choi, J.; Hong, B. H. Large-Scale Pattern Growth of Graphene Films for Stretchable Transparent Electrodes. *Nature* **2009**, *457*, 706–710.
3. Chae, S. J.; Güneş, F.; Kim, K. K.; Kim, E. S.; Han, G. H.; Kim., S. M.; Shin., H.; Yoon, S.; Choi, J.; Park, M. H.; et al. Synthesis of Large-Area Graphene Layers on Poly-Nickel Substrate by Chemical Vapor Deposition: Wrinkle Formation. *Adv. Mater.* **2009**, *21*, 2328–2333.
4. Güneş, F.; Han, G. H.; Kim, K. K.; Kim, E. S.; Chae, S. J.; Park, M. H.; Jeong, H. K.; Lim, S. J.; Lee, Y. H. Large Area Graphene-Based Flexible Transparent Conducting Films. *NANO* **2009**, *4*, 83–90.
5. Gomez De Arco, L.; Zhang, Y.; Kumar, A.; Zhou, C. Synthesis, Transfer, and Devices of Single- and Few-Layer Graphene by Chemical Vapor Deposition. *IEEE Trans. Nanotechnol.* **2009**, *8*, 135–138.
6. Li, X.; Cai, W.; An, J.; Kim, S.; Nah, J.; Yang, D.; Piner, R.; Velamakanni, A.; Jung, I.; Tutuc, E.; et al. Large-Area Synthesis of High-Quality and Uniform Graphene Films on Copper Foils. *Science* **2009**, *324*, 1312–1314.
7. Liu, L.; Ryu, S.; Tomasik, M. R.; Stolyarova, E.; Jung, N.; Hybertsen, M. S.; Strigerwald, M. L.; Brus, L. E.; Flynn, G. W. Graphene Oxidation: Thickness-Dependent Etching and Strong Chemical Doping. *Nano Lett.* **2008**, *8*, 1965–1970.
8. Datta, S. S.; Strachan, D. R.; Khamis, S. M.; Charlie Johnson, A. T. Crystallographic Etching of Few-Layer Graphene. *Nano Lett.* **2008**, *8*, 1912–1915.
9. Campos, L. C.; Manfrinato, V. R.; Sanchez-Yamagishi, J. D.; Kong, J.; Jarillo-Herrero, P. Anisotropic Etching and Nanoribbon Formation in Single-Layer Graphene. *Nano Lett.* **2009**, *9*, 2600–2604.
10. Novoselov, K. S.; Geim, A. K.; Morozov, S. V.; Jiang, D.; Zhang, Y.; Dubonos, S. V.; Grigorieva, I. V.; Firsov, A. A. Electric Field Effect in Atomically Thin Carbon Films. *Science* **2004**, *306*, 666–669.
11. Zhang, Y.; Tan, Y.; Stormer, H. L.; Kim, P. Experimental Observation of The Quantum Hall Effect and Berry's Phase in Graphene. *Nature* **2005**, *438*, 201–204.
12. Zhou, Y.; Bao, Q.; Varghese, B.; Tang, L. A. L.; Tan, C. K.; Sow, C.-H.; Loh, K. P. Microstructuring of Graphene Oxide Nanosheets Using Direct Laser Writing. *Adv. Mater.* **2010**, *22*, 67–71.
13. Ferrari, A. C.; Meyer, J. C.; Scardaci, V.; Casiraghi, C.; Lazzeri, M.; Mauri, F.; Piscanec, S.; Jiang, D.; Novoselov, K. S.; Roth, S.; et al. Raman Spectrum of Graphene and Graphene Layers. *Phys. Rev. Lett.* **2006**, *97*, 187401.
14. Blake, P.; Hill, E. W.; Castro Neto, A. H.; Novoselov, K. S.; Jiang, D.; Yang, R.; Booth, T. J.; Geim, A. K. Making Graphene Visible. *Appl. Phys. Lett.* **2007**, *91*, 063124.
15. Jung, I.; Pelton, M.; Piner, R.; Dikin, D. A.; Stankovich, S.; Watcharotone, S.; Hausner, M.; Ruoff, R. S. Simple Approach for High-Contrast Optical Imaging and Characterization of Graphene-Based Sheets. *Nano Lett.* **2007**, *7*, 3569–3575.
16. Wang, Y. Y.; Ni, Z. H.; Ting, Y.; Shen, Z. X.; Wang, H. M.; Wu, Y. H.; Chen, W.; Wee, A. T. S. Raman Studies of Monolayer Graphene: The Substrate Effect. *J. Phys. Chem. C* **2008**, *112*, 10637–10640.
17. Gao, L.; Ren, W.; Li, F.; Cheng, H. Total Color Difference for Rapid and Accurate Identification of Graphene. *ACS Nano* **2008**, *2*, 1625–1633.
18. Anders, H. *Thin Films in Optics*; Focal: London, 1967; p 18.
19. Abergel, D. S. L.; Russell, A.; Fal'ko, V. I. Visibility of Graphene Flakes on a Dielectric Substrate. *Appl. Phys. Lett.* **2007**, *91*, 063125.
20. Falkovsky, L. A.; Pershoguba, S. S. Optical Far-Infrared Properties of a Graphene Monolayer and Multilayer. *Phys. Rev. B* **2007**, *76*, 153410.
21. Casiraghi, C.; Hartschuh, A.; Lidorikis, E.; Qian, H.; Harutyunyan, H.; Gokus, T.; Novoselov, K. S.; Ferrari, A. C. Rayleigh Imaging of Graphene and Graphene Layers. *Nano Lett.* **2007**, *7*, 2711–2717.
22. Roddaro, S.; Pingue, P.; Piazza, V.; Pellegrini, V.; Beltram, F. The Optical Visibility of Graphene: Interference Colors of Ultrathin Graphite on SiO. *Nano Lett.* **2009**, *7*, 2707–2710.
23. Ni, Z. H.; Wang, H. M.; Kasim, J.; Fan, H. M.; Yu, T.; Wu, Y. H.; Feng, Y. P.; Shen, Z. X. Graphene Thickness Determination Using Reflection and Contrast Spectroscopy. *Nano Lett.* **2007**, *7*, 2758–2763.
24. Ishigami, M.; Chen, J. H.; Cullen, W. G.; Fuhrer, M. S.; Williams, E. D. Atomic Structure of Graphene on SiO_2. *Nano Lett.* **2007**, *7*, 1643–1648.
25. Tan, P. H.; Deng, Y. M.; Zhao, Q.; Cheng, W. C. The Intrinsic Temperature Effect of The Raman Spectra of Graphite. *Appl. Phys. Lett.* **1999**, *74*, 1818.
26. Calizo, I.; Balandin, A. A.; Bao, W.; Miao, F.; Lau, C. N. Temperature Dependence of The Raman Spectra of Graphene and Graphene Multilayers. *Nano Lett.* **2007**, *7*, 2645–2649.
27. Sun, K.; Stroscio, M. A.; Dutta, M. Graphite C-Axis Thermal Conductivity. *Superlattices Microstruct.* **2009**, *45*, 60–64.
28. Jang, W.; Chen, Z.; Bao, W.; Lau, C. N.; Dames, C. Thickness-Dependent Thermal Conductivity of Encased Graphene and Ultrathin Graphite. *Nano Lett.* **2010**, *10*, 3909–3913.
29. Chen, Z.; Jang, W.; Bao, W.; Lau, C. N.; Dames, C. Thermal Contact Resistance between Graphene and Silicon Dioxide. *Appl. Phys. Lett.* **2009**, *95*, 161910.
30. Güneş, F.; Shin, H.-J.; Biswas, C.; Han, G. H.; Kim, E. S.; Chae, S. J.; Choi, J.-Y.; Lee, Y. H. Layer-by-Layer Doping of Few-Layer Graphene Film. *ACS Nano* **2010**, *4*, 4595–4600.
31. Nair, R. R.; Blake, P.; Grigorenko, A. N.; Novoselov, K. S.; Booth, T. J.; Stauber, T.; Peres, N. M. R.; Geim, A. K. Fine Structure Constant Defines Visual Transparency of Graphene. *Science* **2008**, *320*, 1308.
32. Mak, K. F.; Sfeir, M. Y.; Wu, Y.; Lui, C. H.; Misewich, J. A.; Heinz, T. F. Measurement of The Optical Conductivity of Graphene. *Phys. Rev. Lett.* **2008**, *101*, 196405.